Traction Force Microscopy of Migrating Normal and H-ras Transformed 3T3 Fibroblasts

Steven Munevar,* Yu-li Wang,* and Micah Dembo†

*Department of Physiology, University of Massachusetts Medical School, Worcester, Massachusetts 01605, and †Department of Biomedical Engineering, Boston University, Boston, Massachusetts 02215 USA

ABSTRACT Mechanical interactions between cell and substrate are involved in vital cellular functions from migration to signal transduction. A newly developed technique, traction force microscopy, makes it possible to visualize the dynamic characteristics of mechanical forces exerted by fibroblasts, including the magnitude, direction, and shear. In the present study such analysis is applied to migrating normal and transformed 3T3 cells. For normal cells, the lamellipodium provides almost all the forces for forward locomotion. A zone of high shear separates the lamellipodium from the cell body, suggesting that they are mechanically distinct entities. Timing and distribution of tractions at the leading edge bear no apparent relationship to local protrusive activities. However, changes in the pattern of traction forces often precede changes in the direction of migration. These observations suggest a frontal towing mechanism for cell migration, where dynamic traction forces at the leading edge actively pull the cell body forward. For H-ras transformed cells, pockets of weak, transient traction scatter among small pseudopods and appear to act against one another. The shear pattern suggests multiple disorganized mechanical domains. The weak, poorly coordinated traction forces, coupled with weak cell-substrate adhesions, are likely responsible for the abnormal motile behavior of H-ras transformed cells.

INTRODUCTION

Complex mechanical interactions take place at cell-substrate and cell-cell adhesion sites. Forces generated at these sites are involved in determining the cell shape and supporting cell migration, allowing cells to perform such important functions as wound healing and embryonic morphogenesis (for a review see Galbraith and Sheetz, 1998). These mechanical interactions likely involve a combination of substrate anchorage and contraction (Lauffenburger and Horwitz, 1996; Elson et al., 1997; Sheetz et al., 1998). Counter forces exerted by the substrate onto cells then cause the cell or part of it to move forward. By coordinating the magnitude of forces and the strength of adhesions in different regions, the cell is able to extend or migrate in a specific direction (Lauffenburger and Horwitz, 1996; Elson et al., 1997; Sheetz et al., 1998).

To address the mechanism of cell locomotion, it is important to determine the spatial and temporal pattern of cell-cell and cell-substrate mechanical interactions. For many decades cultured fibroblasts have been used as a model for studying cell migration and cell-substrate interactions. In addition, fibroblasts transfected with oncogenes such as H-ras manifest typical cancer phenotypes such as anchorage-independent growth and metastasis (Bondy et al., 1985; Varani et al., 1986; Brown et al., 1989; Egan et al., 1987; Byers et al., 1991), making them ideal candidates for studying the effects of oncogenic transformation on cell-substrate mechanical interactions.

Traction stresses generated by fibroblasts were first investigated using thin silicone rubber substrata (Harris et al., 1980; Leader et al. 1983), where wrinkles appear as a result of compression and stretching. However, because wrinkling is an inherently nonlinear and chaotic process, there is no known theoretical method for predicting the wrinkles that will occur in a substratum as a result of complex loading. Although significant efforts have been made to develop alternative methods for force detection (Galbraith and Sheetz, 1997), and to improve the silicone rubber technique for better quantification and versatility (Burton and Taylor, 1997; Oliver et al., 1998; Burton et al., 1999), quantitative mapping of traction stresses during fibroblast migration has yet to be accomplished.

In the present study we have acquired images depicting the dynamics of various characteristics of the forces at the cell-substratum interface. The new approach, referred to as traction force microscopy, is based on our recently developed polyacrylamide substrates (Wang and Pelham, 1998) and on the application of computational procedures to convert measurements of substrate deformation into a maximum likelihood estimate of the traction stresses (Dembo and Wang, 1999). Improvements in data collection, analysis, and rendering have now made it possible to generate time-lapse images and shear fields of traction stress at a high spatial and temporal resolution. We have applied this approach to analyze the dynamics of cell-substrate mechanical interactions for normal and transformed cells. Our results indicate that normal NIH 3T3 cells exert strong, dynamic propulsive forces within a discrete zone near the leading edge, which are likely responsible for towing the cell body forward during cell migration. In contrast, H-ras

Received for publication 30 May 2000 and in final form 11 January 2001.

Address reprint requests to Dr. Yu-li Wang, University of Massachusetts Medical School, 377 Plantation Street, Room 327, Worcester, MA 01605. Tel.: 508-856-8781; Fax: 508-856-8774; E-mail: yuli.wang@umassmed.edu.

0006-3495/01/04/1744/14 $2.00

transformed cells display transient, weak, and poorly coordinated traction stress all along the cell perimeter. Our observations allow us to propose a frontal towing model for fibroblast migration.

MATERIALS AND METHODS

Preparation of polyacrylamide substrates

Thin sheets of polyacrylamide gel were prepared from acrylamide (Bio-Rad, Richmond, CA; 40% w/v) and *N*,*N*-methylene-bis-acrylamide (BIS, Bio-Rad; 2% w/v) and adhered to activated coverslips, as described in detail previously (Wang and Pelham, 1998). All the substrates used in this study contained 5% acrylamide, 0.1% BIS, and 1:100 dilution of fluorescent latex beads (0.2-μm FluoSpheres, Molecular Probes, Eugene, OR). A 15-μl volume of the acrylamide solution was spread onto the surface of an activated large coverslip (45 $\times$ 50 mm) and contained under a 22-mm-diameter circular coverslip. Type I collagen was covalently attached to the surface of the polyacrylamide gel using photoactivatable heterobifunctional reagent sulfosuccinimidyl 6 (4-azido-2-nitrophenyl-amino) hexanoate (sulfo-SANPAH), as described previously (Wang and Pelham, 1998).

Characterization of substrates

Steady-state thickness of the polyacrylamide sheets at 37°C was estimated to be ~75 μm, by focusing a microscope with a calibrated focusing knob from the glass surface to the surface of the polyacrylamide gel. Young's modulus of the polyacrylamide sheets was determined based on the Hertz theory, similar to the method used in atomic force microscopy (Radmacher et al., 1992). Briefly, a steel ball (0.64-mm diameter, 7.2 g/cm^3; Microball Co., Peterborough, NH) was placed onto the polyacrylamide sheets embedded with fluorescent beads. The resulting indentation was measured by following the vertical position of surface fluorescent beads under the center of the steel ball with the microscope focusing mechanism. Young's modulus was calculated as $Y = 3(1 - \nu^2)^2 f^2/4d^{3/2}r^{1/2}$, where f is the buoyancy-corrected weight of the steel ball, d is the indentation of the substrate, r is the radius of the steel ball, and ν is the Poisson ratio of polyacrylamide assumed to be 0.3 in this study (Li et al., 1993). This method yielded a Young's modulus of 28 $\times$ 10^3 N/m^2 for the substrates.

Cell culture and microscopy

Polyacrylamide substrates were equilibrated with the culture medium for approximately 30 min at 37°C. NIH 3T3 cells and a metastatic line of H-ras transformed NIH 3T3 cells, PAP2, were kindly provided by Dr. Ann Chambers (Bondy et al., 1985; Hill et al., 1988). The cells were cultured in Dulbecco's modified Eagle's medium (Sigma, St. Louis, MO), supplemented with 10% donor calf serum (JHR Biosciences, Lenexa, KS), 2 mM L-glutamine, 50 μg/ml streptomycin, and 50 U/ml penicillin (Gibco-BRL, Gaithersburg, MD).

Phase images of cells, fluorescent images of substrates-embedded beads, and combined phase/fluorescence images were collected with a Zeiss 40X, NA 0.65 Achromat phase objective on a Zeiss IM-35 microscope. The microscope was equipped with a stage incubator. Bead images of relaxed substrates were collected at the end of time-lapse recordings by microinjecting cells with Gc-globulin, a known actin cytoskeleton inhibitor (Van Baelen et al., 1980; Goldschmidt-Clermont et al., 1985; Lee and Galbraith, 1992). All images were collected with a cooled CCD camera (TE/CCD-576EM; Princeton Instruments, Trenton, NJ) and processed for background subtraction using custom programs.

Calculation and rendering of traction magnitude and shear

Deformation of the substrate by cultured cells was determined relative to the relaxed substrate, based on pattern recognition using a cross-correlation algorithm. Briefly, a force-loaded bead image was first divided into small square areas. The computer program then tried to match the bead pattern in each small square against the pattern in different regions of the null-force image, searching for a best match. Deformation vectors were then drawn from the position in the null-force image to the position in the force-loaded image with the best match. The degree of match was scored with a normalized cross-correlation equation, which yielded a value of 1 for a perfect match and 0 for no similarity. No vector was assigned if this value fell below a user-defined threshold. In regions where the deformation was larger than one pixel, additional vectors were generated at a progressively shortened distance from each other to provide a higher density of data. The size of the square, the distance for the pattern search, and the threshold for positive identification were determined empirically, to generate an optimal set of vectors that matched visual assessment of substrate displacement when the null and force-loaded images were displayed in quick succession. Cell boundaries were drawn manually using phase images and a custom interactive program. Coordinates defining the deformation field and cell boundary were then input into a supercomputer and analyzed with a maximum likelihood algorithm, which generates traction vectors at pre-assigned nodes throughout the cell (Dembo and Wang, 1999). Average compressive stress was calculated by averaging the absolute values of stress vectors projected onto specified directions. The projection was obtained by multiplying the magnitude of the vector with the cosine of the angle between the vector and the direction of projection. The traction magnitude, *mag*, and shear, *shr*, are defined as follows:

$$mag(\mathbf{T}) = |\mathbf{T}| \equiv [T_x^2 + T_y^2]^{1/2} \quad (1)$$

$$shr(\mathbf{T}) \equiv [2(\partial_x T_x)^2 + (\partial_y T_x + \partial_x T_y)^2 + 2(\partial_y T_y)^2]^{1/2}, \quad (2)$$

where $\mathbf{T} = [T_x(x, y), T_y(x, y)]$ is the continuous field of traction vectors underlying the cell.

One should notice that $shr(\mathbf{T})$ essentially measures the magnitude of the spatial derivatives of the traction field with a combination of derivatives. Spatial derivatives of the traction field are of biological interest because, potentially, they can identify locations where there are sudden qualitative changes in contractility or adhesion. For purposes of comparing such changes across different cells and between different regions of the same cell, one is mainly interested in the changes relative to the prevailing background of traction. Thus, it is useful to normalize the shear fields by dividing with the corresponding traction magnitude. The ratio will be referred to as normalized shear. Pseudo-color images were obtained by first determining the magnitude of the scalar or vector at each pixel within the cell boundary by interpolation and then converting the magnitude into different red-green-blue color combinations.

RESULTS

Traction force microscopy

The basic approach for mapping traction stresses has been described in Dembo and Wang (1999). The method is based on the use of flexible polyacrylamide substrates, coated with extracellular matrix proteins (type I collagen in the present study) for cell adhesion and embedded with fluorescent beads for tracking the deformation as a result of exerted forces. Several modifications were made to improve the spatial resolution and to facilitate the visualization of calculated results. First, substrate stiffness was optimized for

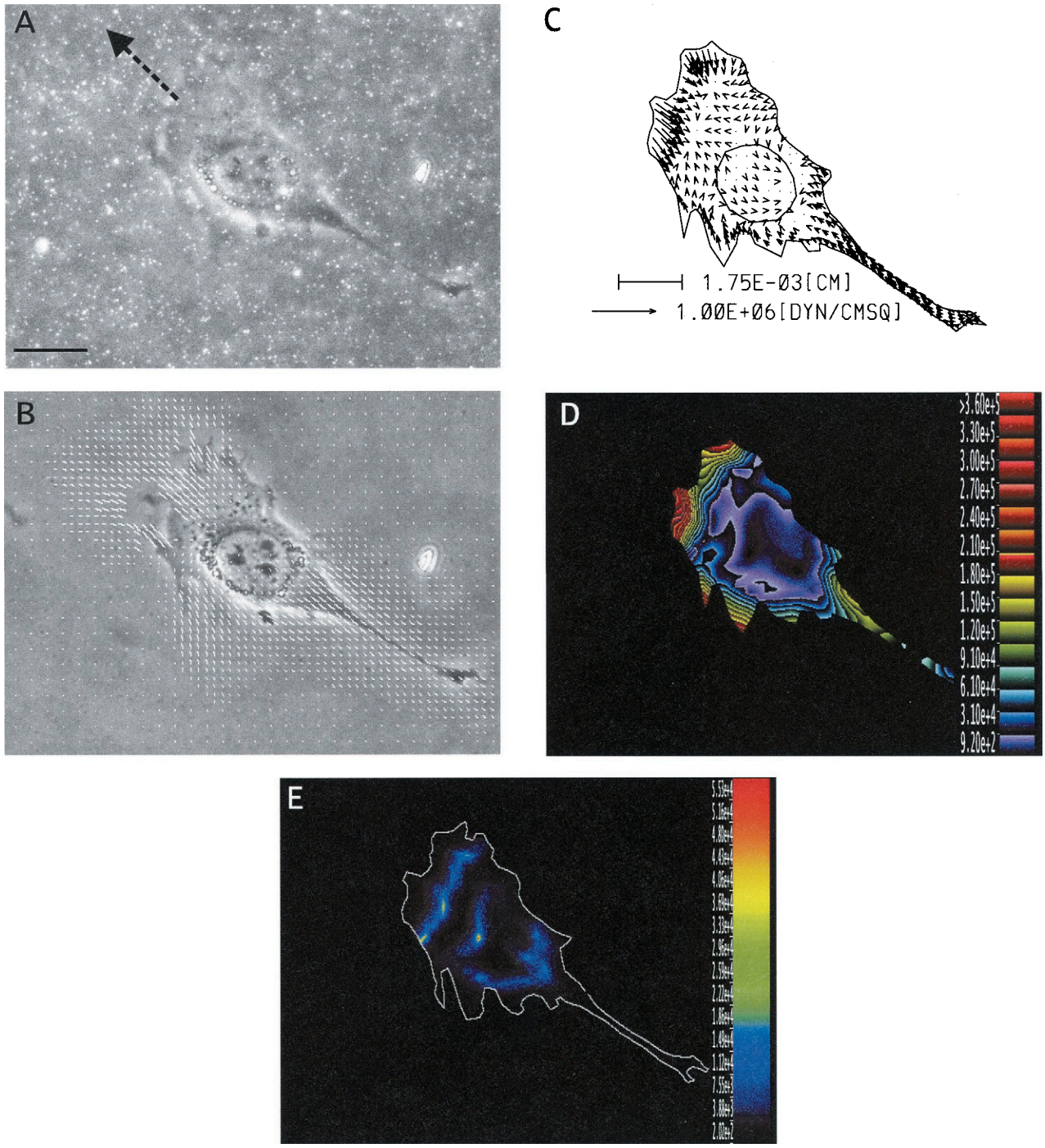

FIGURE 1 Traction force microscopy. (*A*) Fluorescent microspheres embedded in polyacrylamide substrates, used for the detection of substrate surface deformation as a result of forces exerted by a NIH 3T3 fibroblast. The image was recorded with simultaneous illumination for phase contrast and epi-fluorescence. Arrow indicates the direction of cell migration. (*B*) Deformation vectors, plotted over the phase image of the cell. Deformation was determined by comparing the distribution of microspheres before and after force relaxation. Regions devoid of vectors either contained few fluorescent beads or went out of focus as a result of traction. (*C*) Field of traction stresses, shown as vectorial arrows within the boundary of the cell. (*D*) Field of traction stresses, rendered as a color image after mapping the magnitude of stress into different colors that range from violet (9.20×10^2 dyn/cm^2) to red ($\geq 3.60 \times 10^5$ dyn/cm^2). The segmented scheme of pseudo-color mapping, as shown along the right edge, allowed the visualization of both the magnitude of stress and the iso-magnitude contours. (*E*) Normalized shear of traction that ranges from violet (2.02×10^2 cm^{-1}) to red (5.53×10^4 cm^{-1}), reflecting the local complexity of traction forces. Areas of uniformly low shear most likely represent mechanically integrated domains. Bands of high shear most likely represent boundaries between these domains. Scale bar, 20 μm.

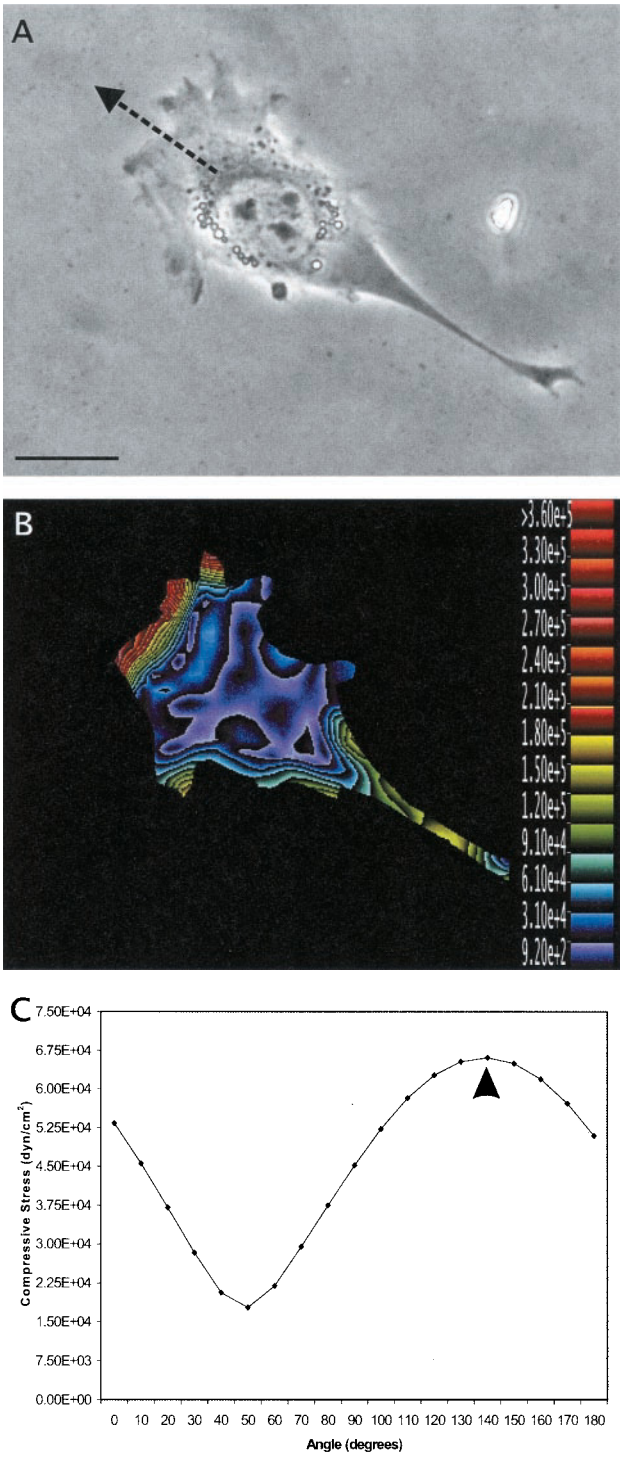

FIGURE 2 Spatial organization of traction stress generated by a migrating normal 3T3 fibroblast. (*A*) Phase contrast image of a migrating normal 3T3 fibroblast. The cell showed a well-defined leading edge and trailing edge during migration. Arrow indicates the direction of cell migration. (*B*) Magnitude of traction stress rendered as a color image, with traction stress ranging from violet (9.20×10^2 dyn/cm^2) to red ($\geq 3.60 \times 10^5$ dyn/cm^2). Strong tractions, denoted in red, were constrained to a thin band along the leading edge of the cell. (*C*) Angular distribution of average compressive stress. Arrowhead denotes the orientation of the long axis of the cell. Scale bar, 20 μm.

the detection of deformation by NIH 3T3 cells, by systematically adjusting the concentrations of acrylamide and bisacrylamide until the maximal traction generated 10–15 pixels of bead displacement. Too stiff a substrate yielded small deformation and large errors; too soft a substrate caused problems with maintaining the plane of focus. Second, the concentration of fluorescent beads was increased by 50–100% (Fig. 1 *A*), which minimized areas devoid of fluorescent marker beads and allowed the generation of a higher density of deformation vectors. Third, deformation was analyzed not by tracking individual beads but by pattern recognition (see Materials and Methods). This allowed a more uniform distribution of deformation vectors. To further increase the amount of useful information, the density of deformation vectors was increased automatically where significant bead displacements were found by generating additional vectors at a progressively shorter distance from each other (Fig. 1 *B*). Calculated traction stresses were displayed either as arrows (Fig. 1 *C*) or as pseudo-color images of the magnitude (*mag*(**T**); Fig. 1 *D*). The scheme of pseudo-color, shown in Fig. 1 *D*, sacrifices directional information of the vectors but facilitates the visualization of magnitudes and iso-magnitude contours.

One major advance in the current study is our ability to obtain time-lapse sequence of traction forces. The increase in the speed of data processing makes it practical to collect data at short intervals, to analyze the traction maps frame by frame, and to render the pseudo-color images as motion pictures. We have currently achieved a temporal resolution of up to ~40 s and an estimated spatial resolution of 3–4 μm, which are more than adequate for studying the relationship between traction forces and the slow migration of 3T3 cells. Furthermore, local protrusions were on average ~9 μm in diameter, with each cycle lasting on average for 55 s ($\pm$39 s SD). Thus, it is also practical to address the relationship between traction forces and protrusive activities.

In addition to magnitude and direction we have calculated *shr*(**T**), which reflects the local spatial derivative of the traction vectors (see Eq. 2 in Materials and Methods for definition). Because spatial fluctuations in traction are meaningful only in comparison with the average traction in a local area, we found it most informative to normalize *shr*(**T**) against *mag*(**T**) in a pixel-by-pixel fashion (Fig. 1 *E*). Thus, within a region where tractions are relatively constant in proportion to the background, the normalized shear values should be low. Along the boundaries of discrete mechanical domains, the ratio *shr*(**T**)/*mag*(*T*) should be high and unstable. This allows us to detect discrete domains in a cell.

Characteristics of traction forces generated by normal NIH 3T3 cells

Most NIH 3T3 cells underwent steady migration on polyacrylamide substrates, with stable, well-defined leading and trailing edges that persisted for up to 2 h (Fig. 2 *A*). Small

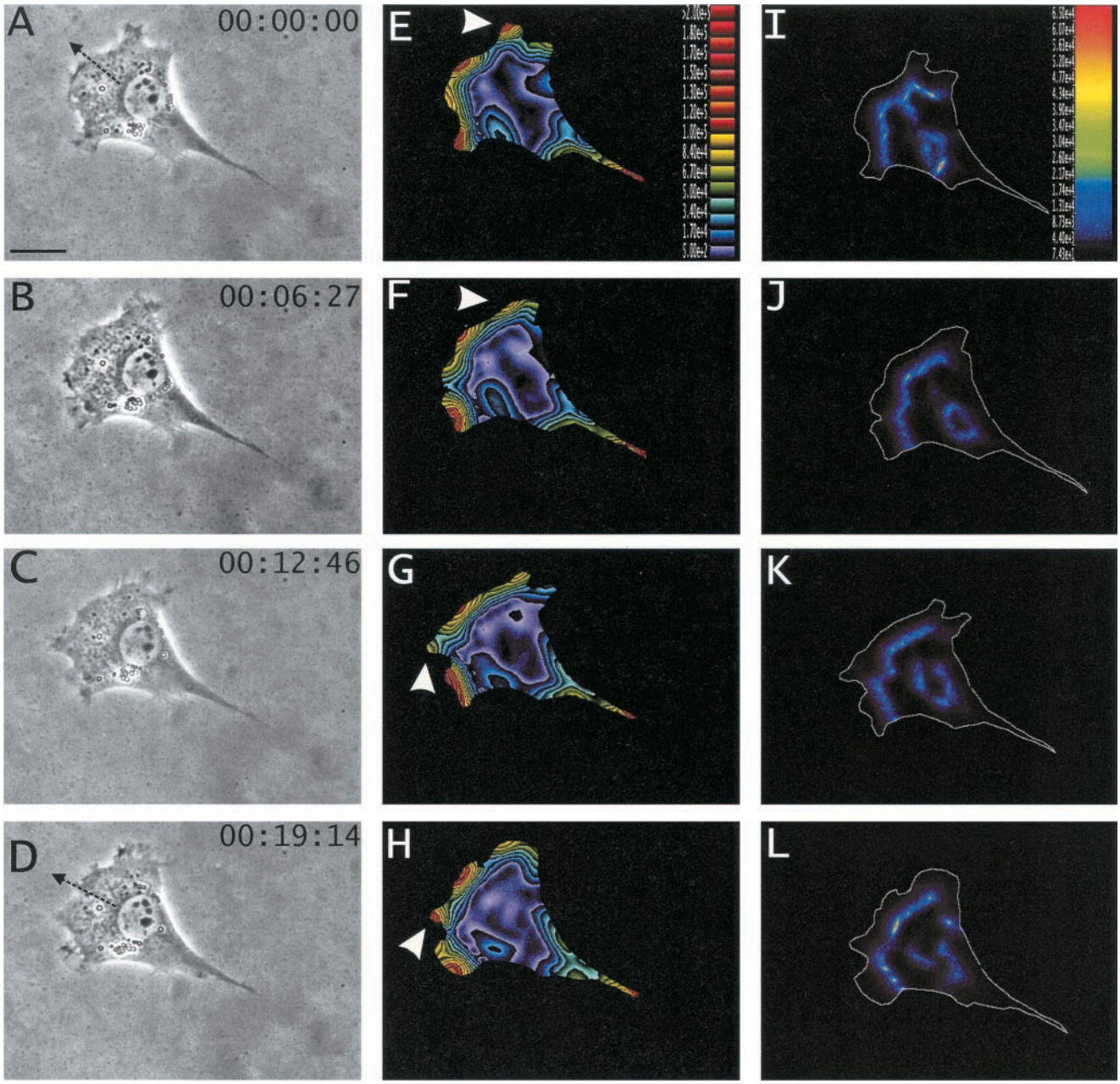

FIGURE 3 Dynamics of traction stress generated by a migrating normal 3T3 fibroblast. (*A–D*) Phase contrast images of a migrating NIH 3T3 fibroblast at $t = 0$, 6 min 27 s, 12 min 46 s, and 19min 14 s. Arrows in *A* and *D* indicate the direction of cell migration at the beginning and end of the experiment respectively. (*E–H*) Color rendering of the corresponding magnitude of traction stress, which ranges from violet (5.00×10^2 dyn/cm^2) to red ($\geq 2.00 \times 10^5$ dyn/cm^2). The strongest tractions, in red, were located at the leading edge as a sharply defined band. These forces were highly dynamic as was the leading edge itself (*white arrowheads*). The trailing end of this cell also showed strong traction. However no significant traction was present around the nucleus. (*I–L*) Color rendering of the corresponding normalized shear that ranges from violet (7.43×10^1 cm^{-1}) to red (6.50×10^4 cm^{-1}). A band of high shear separates the leading edge from the main body of the cell. Scale bar, 20 μm.

protrusions sometimes appeared along the sides (Fig. 1 *D*). These protrusions were short-lived in most cases but occasionally were able to expand and replace an existing leading edge, causing a change in the direction of migration (discussed later). In agreement with our previous studies (Dembo and Wang, 1999; Pelham and Wang, 1999), all the significant traction forces were directed toward the interior of the cell. From the general organization of the traction field, one can conclude that essentially all the propulsive forces for forward migration were concentrated at the leading edge (Figs. 1, *C* and *D* and 2 *B*), although strong foci of retarding traction were sometimes present in the tail region

TABLE 1 Average traction stress for migrating normal NIH 3T3 and H-ras transformed fibroblasts

	Average traction stress (dyn/cm^2)	
Cell number	3T3	Pap2
1	1.07×10^4	1.43×10^4
2	1.81×10^4	7.80×10^3
3	2.67×10^4	9.95×10^3
4	4.17×10^4	7.81×10^3
5	3.69×10^4	
6	8.08×10^4	
7	2.21×10^4	
8	1.67×10^4	
9	1.94×10^4	
Mean	3.03×10^4	9.97×10^3
SD	2.13×10^4	3.06×10^3

(Fig. 3). The overall average of traction stresses was 3.03×10^4 dyn/cm^2 with a standard deviation of 2.13×10^4 dyn/cm^2 (Table 1). When average compressive stresses were calculated along different directions, we found that there was a strong bias along the long axis of a steadily migrating 3T3 cell (Fig. 2 *C*).

Time-lapse analysis revealed that, in most cases, cells undergoing steady migration maintained a band of strong traction forces at the lamellipodium. Sub-regions within the leading lamellipodium showed large spatial and temporal variations in traction forces. Pockets of strong forces appeared and disappeared constantly throughout this region, with each pulse of traction lasting on average 24 min (Fig. 3, *E–H*). Transient strong traction forces, comparable in magnitude to those in the lamellipodia, were also found at lateral protrusions. However, they covered a smaller area and appeared as isolated pulses rather than recurring events.

Further insights were provided by rendering images of normalized shear values of the stress (Fig. 3, *I–L*). In cells migrating at steady state, a band of high shear values, as denoted by the bright region in color rendering, was found just behind the lamellipodium, where traction forces dropped sharply in magnitude and reversed in direction. This suggests that the frontal region and the rest of the cell are mechanically distinct domains. The lamellipodium region at times can be divided into multiple small domains separated by regions of high shear. In contrast, normalized shear values in the trailing end were typically low, as denoted by the darkness in color rendering, despite the presence of strong forces there in some cells (Fig. 3, *E* and *I*). The rest of the cell body can be grouped into a few large domains; a band of significant shear was typically found beneath the nucleus, where weak forces from the two lateral sides collided.

Relationship between traction forces and cell migration

To determine the role of traction forces in cell migration, we first examined the relationship between frontal traction stress and local protrusive activities. As shown in Fig. 4, *A–D*, during cell migration membrane protrusion and retraction occurred rapidly and dynamically along the leading edge. These events showed no apparent correlation with the appearance or disappearance of local traction forces (Fig. 4).

A second possibility is that frontal traction is related to the migration of the cell body, as suggested by the tight correlation between the distribution of forces and the polarity of the cell (Fig. 2). We have therefore focused on cells that changed the direction of migration during the period of observation ($N = 9$). As shown in Fig. 5, redistribution of traction forces can take place well in advance of the change in cell polarity. The original leading edge maintained its ruffling activity for an extended period of time with no significant local traction forces, whereas strong sustained traction forces started to develop in the region that subsequently became the leading edge (Fig. 5, *D–F*). These observations support the notion that the spatial and temporal pattern of traction forces dictates the direction of cell migration.

Traction forces generated by H-ras transformed NIH 3T3 cells

To determine the impact of oncogenic transformation on traction forces, we used an H-ras transformed clone of NIH 3T3 cells (PAP2 cells), originally selected for their ability to metastasize in chick embryos (Bondy et al., 1985; Egan et al., 1987). Morphologically, PAP2 cells were poorly polarized, exhibiting multiple transient protrusions instead of a well-defined lamellipodium (Fig. 6 *A*). Cell migration was affected by these protrusions, which appeared to drag the cells in a disorganized fashion. These cells migrated with a poor directional stability yet at a higher average speed of 0.31 μm/min, as compared with 0.19 μm/min for normal cells.

Although the traction stresses exerted by PAP2 cells were generally directed inward as in normal cells, significant forces were found only in small pockets near the tip of multiple scattered protrusions (Fig. 6 *B*). Furthermore, there was no region that could be unambiguously identified as the trailing end, based on either the morphology or force characteristics. The average traction magnitude, 9.97×10^3 dyn/cm^2 with a standard deviation of 3.06×10^3 dyn/cm^2 (Table 1), was markedly reduced as compared with that for normal cells ($p < 0.02$). In addition, traction forces generated by PAP2 cells showed no angular directionality, in contrast to what was observed in normal cells (Fig. 6 *C*).

Time-lapse analysis of the traction stress indicated that the distribution of forces in PAP2 cells was very unstable (Fig. 7, *E–H*). Although the average duration of each traction event, 22–23 min, was similar to that in normal cells, no region was able to develop a concentration of traction forces or to maintain the activity for any extended period of time.

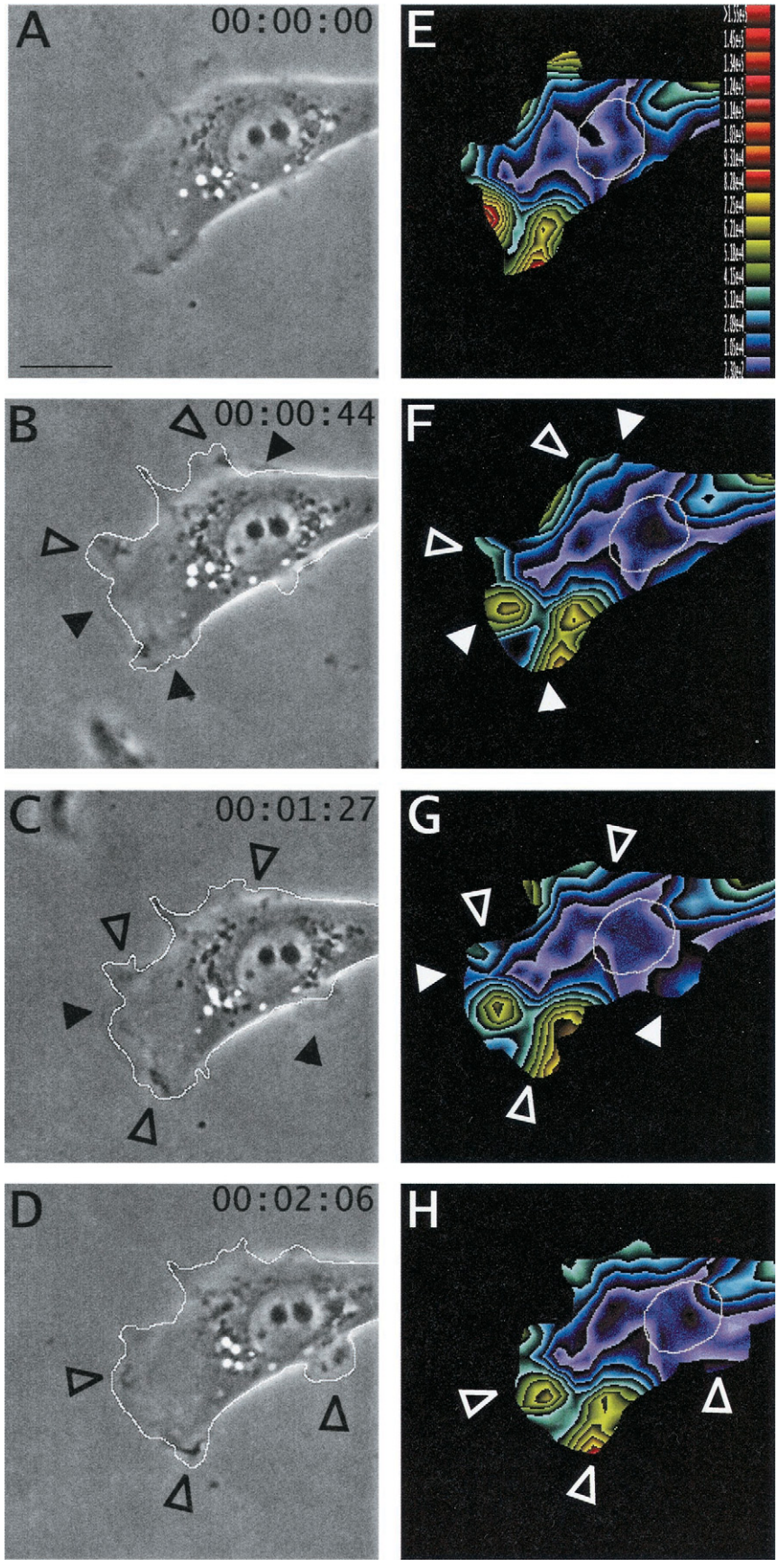

FIGURE 4 Membrane protrusion and traction stress at the leading edge of a migrating normal 3T3 fibroblast. (*A–D*) Phase contrast images of a migrating NIH 3T3 fibroblast at $t = 0$, 44 s, 1 min 27 s, and 2 min 6 s. The outline of the cell at the previous time point is drawn as white lines in panels *B–D*. Open arrowheads indicate the sites of retraction and closed arrowheads identify the sites of protrusion. (*E–H*) Color rendering of the corresponding magnitude of traction stress, which ranges from violet (2.30×10^2 dyn/cm^2) to red ($\geq 1.55 \times 10^5$ dyn/cm^2). Arrowheads indicate protrusive/retraction activities as in phase images. Lamellipodial protrusion/retraction can take place both during the peak of local traction stress and during a period without significant traction forces. Circular white traces indicate the position of the nucleus in *E–H*. Scale bar, 20 μm

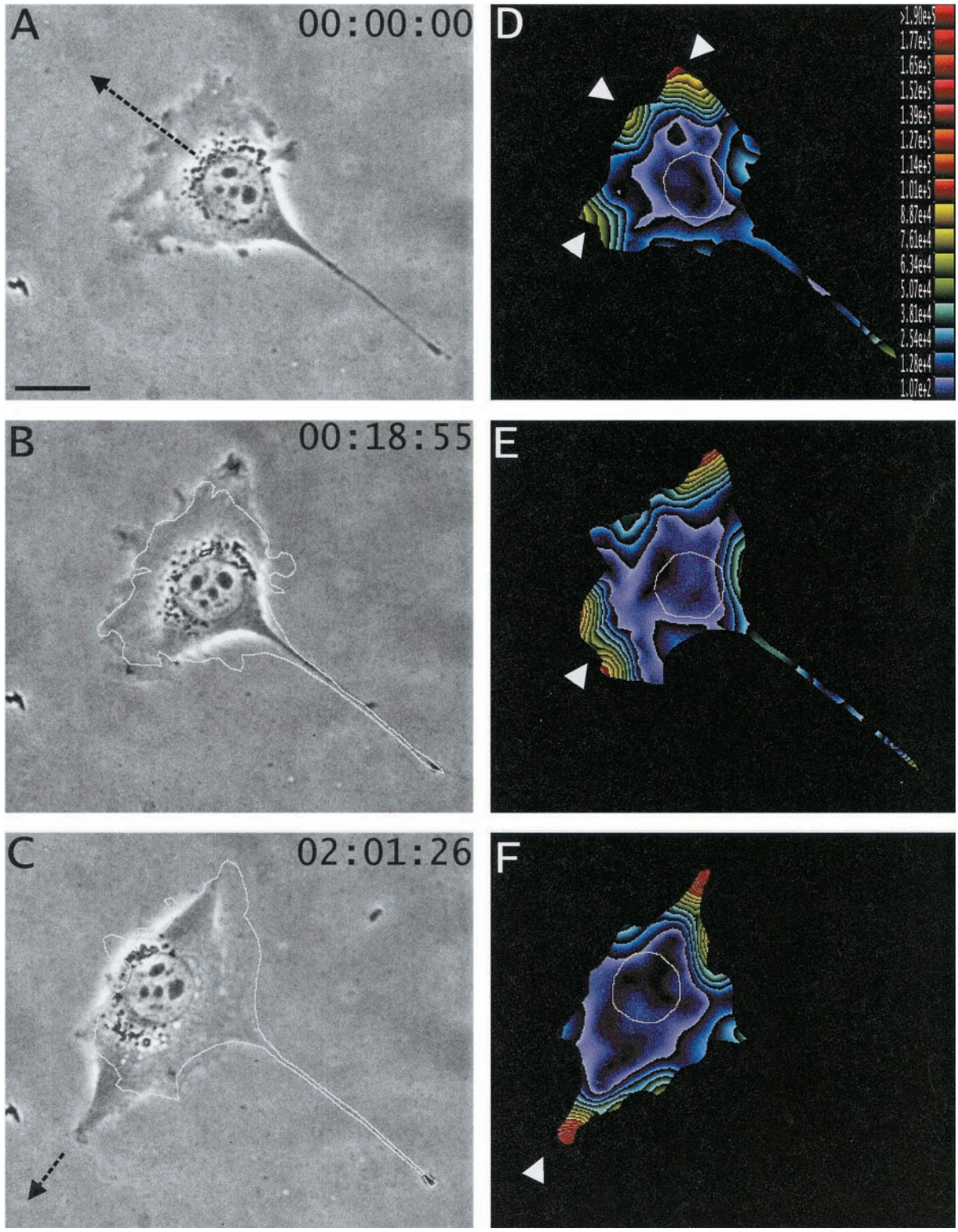

FIGURE 5 Traction stress generated by a migrating normal 3T3 fibroblast during directional change. (*A–C*) Phase contrast images of a migrating NIH 3T3 fibroblast at $t = 0$, 18 min 55 s, and 121 min 26 s. Arrows in *A* and *C* indicate the direction of cell migration. The outline of the cell at the previous time point is drawn as white lines in *B* and *C*. The cell shows a 90° change in direction. (*D–F*) Color rendering of the corresponding magnitude of traction stress, which ranges from violet (1.07×10^2 dyn/cm^2) to red ($\geq 1.90 \times 10^5$ dyn/cm^2). White arrowheads identify pockets of strong traction stress. Changes in the overall distribution of traction stress become apparent before the cell changes its polarity (*E*). One end of the cell shows strong traction before developing into a leading edge (*E*, *arrowhead*). Some protrusive activities persist at the original leading edge whereas the local traction stress drops to a very low level (*B* and *E*). Circular white traces indicate the position of the nucleus in *D–F*. Scale bar, 20 μm

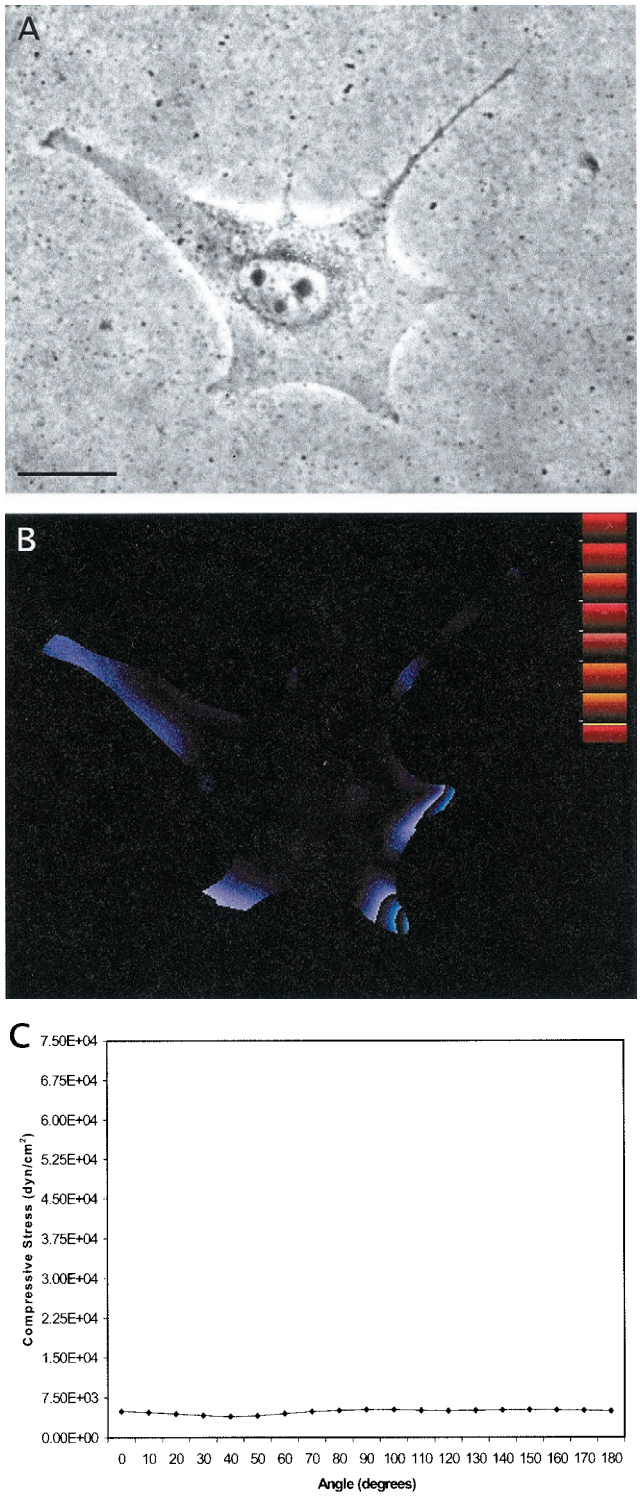

FIGURE 6 Spatial organization of traction stress generated by a migrating H-ras transformed NIH 3T3 fibroblast. (*A*) Phase contrast image of a migrating H-ras transformed NIH 3T3 fibroblast. Arrow indicates the direction of cell migration. Note the absence of a well-defined leading edge and trailing edge. (*B*) Color rendering of the corresponding magnitude of traction stress, which ranges from violet (9.20×10^2 dyn/cm^2) to red ($\geq 3.60 \times 10^5$ dyn/cm^2), using the same color-mapping scheme as that for normal cells in Fig. 2. Compared with normal fibroblasts, the overall magnitude of traction stress is markedly reduced, as is the spatial organization. (*C*) Angular distribution of average compressive stress, showing the lack of angular asymmetry in contrast to what is seen in Fig. 2. Scale bar, 20 μm.

In contrast to normal cells where a band of high shear was present at the base of lamellipodia, pockets or bands of high shear values scattered in numerous locations and migrated chaotically (Fig. 7, *I–L*). Therefore, transformed cells were able to develop transient protrusions and tractions but were unable to turn them into a stable lamellipodium.

DISCUSSION

We have developed a new imaging technique, traction force microscopy, to map mechanical forces generated by normal and H-ras transformed fibroblasts. This approach combines flexible substrates, digital imaging, and computation to deconvolve substrate deformation into the distribution of mechanical forces. The use of an automatic deformation determination algorithm, the improved spatial and temporal resolution, and the color rendering of traction parameters have greatly increased the efficiency and power of this approach beyond its predecessor or other force mapping techniques (Dembo and Wang, 1999). New features in the present study include time-lapse analysis of traction field relative to cell migration, the generation of shear pattern for identifying discrete mechanical domains, and the elucidation of differences in substrate mechanical interactions of normal versus transformed cells.

Traction forces exerted by normal cells on the substrate: a frontal towing model for 3T3 cell migration

Our results showed that all traction forces generated by NIH 3T3 cells are pointed toward the center of the cell, with the strongest forces concentrating near the very tip of the lamellipodia and dropping precipitously toward the central region. These observations generally agree with what we reported with Swiss 3T3 cells using static methods (Dembo and Wang, 1999; Pelham and Wang, 1999). Furthermore, new results from this study indicate that traction at the leading edge does not correlate directly with local protrusive activities, but with the overall direction of cell migration. As shown in Fig. 2 *C*, although traction forces are generated at scattered sites, the direction of maximal compressive stress generally lies parallel to the long axis of steadily migrating cells. In addition, the distribution of traction forces changes before changes in the direction of cell migration. Protrusive regions that show persistent traction forces develop into dominant lamellipodia, whereas those with only transient traction activities retract quickly. Therefore, the polarity of cell migration is not determined

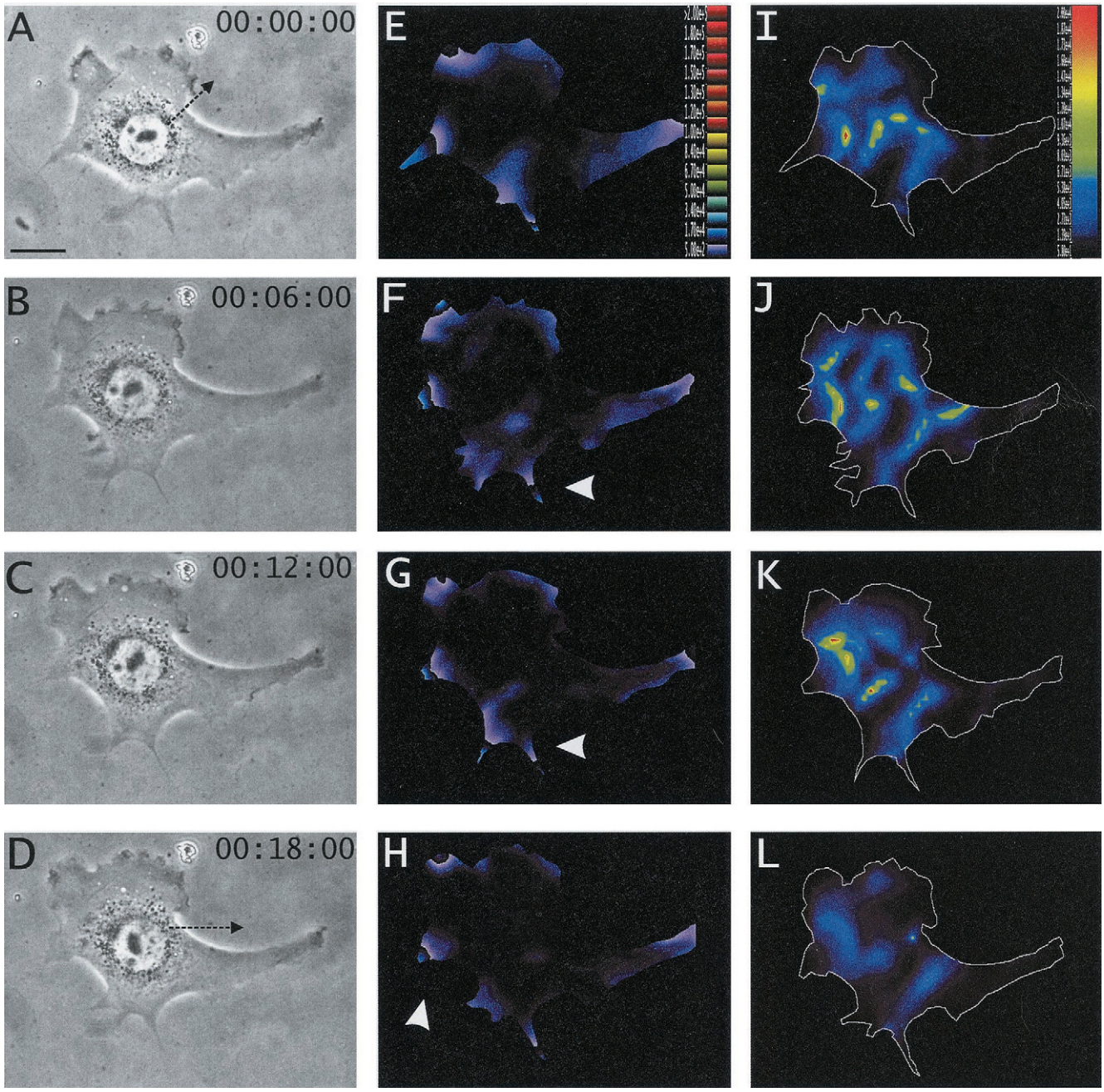

FIGURE 7 Dynamics of traction stress generated by a migrating H-ras transformed NIH 3T3 fibroblast. (*A–D*) Phase image of a migrating H-ras transformed NIH 3T3 fibroblast at $t = 0$, 6 min, 12 min, and 18 min. Arrows in *A* and *D* indicate the direction of cell migration. Note the multiple leading-edge-like protrusions. (*E–H*) Color rendering of the corresponding magnitude of traction stress, which ranges from violet (5.00×10^2 dyn/cm^2) to red ($\geq 2.00 \times 10^5$ dyn/cm^2) using the same color scheme as in Fig. 3. The magnitude of traction was sharply reduced as compared with that in normal cells. In addition, traction stress was exerted at small, highly unstable pockets along the perimeter of the cell (*arrowheads*). (*I–L*) Color rendering of the corresponding normalized shear that ranges from violet (5.80×10^1 cm^{-1}) to red (2.00×10^4 cm^{-1}). The unstable, complex pattern of shear bands suggests a mechanically fragmented cell body. Scale bar, 20 μm.

by membrane protrusion per se but by the subsequent development of firm adhesion and traction forces, which may play a role in sustaining the local protrusive activities and in pulling the cell body forward. This mechanism allows the cell to send local protrusions in various directions to probe the environment while maintaining a steady course of movement.

In addition, the shear field of traction indicates that normal cells can be divided into mechanically discrete segments or zones. The lamellipodium is separated from the

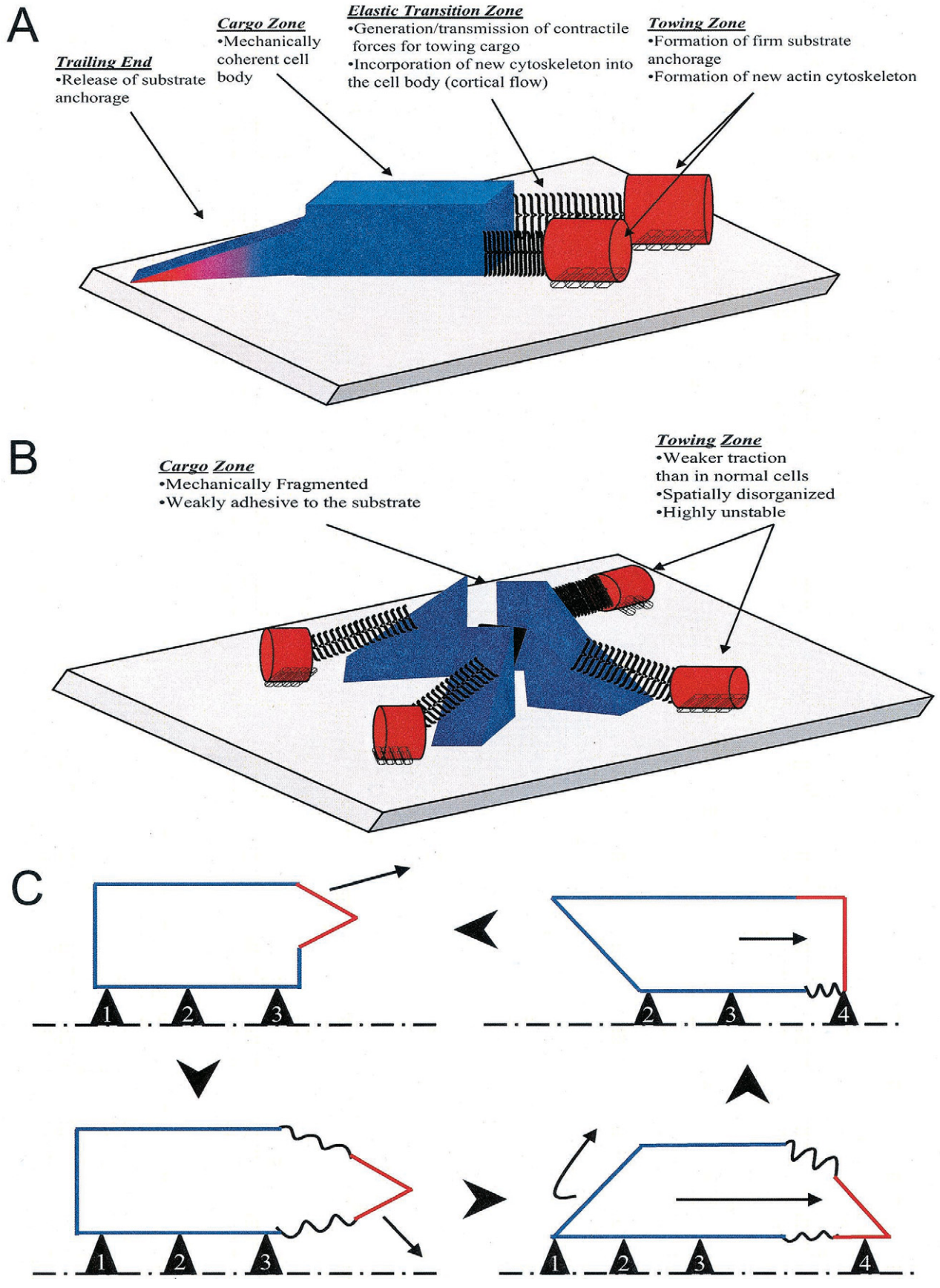
A
Trailing End
•Release of substrate anchorage
Cargo Zone
•Mechanically coherent cell body
Elastic Transition Zone
•Generation/transmission of contractile forces for towing cargo
•Incorporation of new cytoskeleton into the cell body (cortical flow)
Towing Zone
•Formation of firm substrate anchorage
•Formation of new actin cytoskeleton
B
Cargo Zone
•Mechanically Fragmented
•Weakly adhesive to the substrate
Towing Zone
•Weaker traction than in normal cells
•Spatially disorganized
•Highly unstable
C
1
2
3
2
3
4
1
2
3
1
2
3
4

rest of the cell by a high shear zone (Fig. 3). The rest of the cell consists of one or several domains, which generate resisting forces against the forward movement. These dragging forces spread across a large region of the cell and sometimes show a strong focus at the tail. Together, these results can be explained with a frontal towing model for cell migration (Fig. 8, *A* and *C*). We propose that the leading lamellipodium consists of one or more transient towing units, which adhere firmly and transmit strong retrograde forces to the substrate. The body of the cell adheres more weakly to the substrate, allowing it to be dragged forward by the frontal towing zone as a mechanically coherent cargo. The towing zone is connected to the cell body via an elastic transition zone, as suggested by a band of high shear in the lamella region, which facilitates the transmission of contractile forces from the cell body to the leading edge. The generation/transmission of contractile forces in this elastic transition zone, combined with the firm anchorage at the front, provides the forces responsible for towing the cargo. To maintain a steady state, this mechanism must be sustained by the continuous formation of new towing units at the leading edge, driven by the assembly of new actin filaments and adhesion sites (Wang, 1985; Depasquale and Izzard, 1987; Small et al., 1998). Furthermore, the detachment, transport, and incorporation of aged towing zones into the cargo zone likely gives rise to the retrograde flow of membrane and cortical components, commonly observed in the lamella region (Heath, 1983).

This frontal towing model is supported not only by the present results but also by a number of past observations. A similar mechanism has been previously speculated by Harris et al. (1980), based on the compression of silicone substrates behind the leading edge. In addition, the existence of a transition zone between the lamellipodium and the cell body is consistent with the organization of actin and myosin II (Svitkina et al., 1997) and the unique behavior of membrane proteins in this region (Ishihara et al., 1988). The idea that the frontal region contains sufficient components for driving cell migration is further supported by the autonomous movement of small cytoplasmic fragments derived from the lamella (Albrecht-Buehler, 1980; Malawista and DeBoisefleury-Chevance, 1982; Verkhovsky et al., 1999). However, important questions remain concerning the molecular mechanisms for the generation and transmission of mechanical forces. Our previous studies indicated that these forces are generated predominantly by actin-myosin-II-based contractions (Pelham and Wang, 1999). Where the forces are generated and how the contractions are regulated remains unclear. Also of great importance is the characterization of substrate adhesions (DiMilla et al., 1991). Because large focal adhesions are typically localized behind the region of strong traction (Pelham and Wang, 1999), we speculate that small, nascent adhesions at the leading edge are more active in transmitting traction forces. Moreover, because the rate of cell migration is determined by a combination of traction forces and adhesiveness, a complete picture would require the determination of the strength and regulation of cell adhesion. Finally, it is important to note that the pattern of traction forces for 3T3 cells differs significantly from that for fish keratocytes and possibly other cell types such as leukocytes (Oliver and Jacobson, 1999; Burton et al., 1999). Thus, different types of cells, or cells under different conditions or morphologies, may use different mechanisms for their migration.

What went wrong in H-ras transformed 3T3 cells

Previous studies with silicone substrates have indicated drastic reductions in the number of wrinkles generated by transformed fibroblasts (Harris et al., 1981; Leader et al., 1983). However, due to the poor resolution of the approach, it was difficult to determine if the effects were due to weakening of the forces, the disorganization of forces, or rapid changes in the distribution of forces. The present study has identified a number of striking differences between the traction forces of normal and H-ras transformed cells. In H-ras transformed cells the magnitude of traction stresses is reduced as compared with that in normal cells, although the duration of local traction activities at the protrusion remains similar. Furthermore, forces exerted by H-ras transformed cells become radially symmetric and scatter among small

FIGURE 8 Model for the migration of normal and H-ras transformed NIH 3T3 fibroblasts. (*A*) Structural model of normal NIH 3T3 fibroblasts. We propose that normal 3T3 cells consist of three distinct mechanical regions: towing zone, elastic transition zone, and cargo zone. Towing zone is located at the front lamellipodium where propulsive traction forces are exerted on the substrate. It is also the region for the assembly of new actin cytoskeleton. The main body of the cell composes the cargo zone. It is connected to the towing zone through an elastic transition zone, which is located in the lamella region. This transition region serves the important function of generating and/or transmitting the contractile forces for cell migration. In addition, active centripetal cortical flow in this region incorporates new cytoskeleton formed in the towing zone into the cell body. Adhesions under the cargo zone and at the trailing end generate the dragging force and have to be released for sustained cell migration. (*B*) Structural model of H-ras transformed 3T3 fibroblasts. H-ras transformation of 3T3 cells results in the formation of multiple, small towing zones. A combination of multiple towing zones and disorganized elastic transition zones gives rise to complex, unstable traction forces and erratic cell movement. As a result the cargo zone becomes highly fragmented. Weakened adhesions likely account for the increased speed of movement. (*C*) Frontal towing model of 3T3 cell migration, broken down into discrete steps. Triangles represent substrate adhesion sites. Arrows represent the direction of movement relative to the substrate. Waved lines represent the flexible transition zone between the frontal towing zone (red outline) and the cargo zone (blue outline). In reality these steps probably take place simultaneously; i.e., new towing zones are assembled as existing ones are exerting traction forces.

pockets, which likely gives rise to the loss of a defined polarity.

The disorganization of traction forces in transformed cells is further demonstrated by the drastically different shear images. Compared with the shear images of normal cells, those of H-ras transformed cells show multiple small, unstable towing domains along the cell perimeter, with neither an organized front nor a well-defined tail. These disorganized towing domains appear to act against one another, trying to drag the cell body in multiple directions. Combined with the weak substrate adhesion of H-ras transformed cells (Shin et al., 1999), these changes in mechanical activities can easily contribute to the erratic, invasive motile behavior of PAP2 cells.

What might lead to the drastic changes in traction forces in transformed cells? We notice that similar transient protrusions are present in both normal and transformed cells. However, in normal cells lateral protrusions are short lived whereas those along the direction of cell migration amplify into a wide expanse of lamellipodium. Therefore, an attractive possibility is that the polarity in normal cells is maintained by a local positive feedback mechanism that amplifies and maintains adhesion sites and traction activities at the leading edge, and possibly by a distal negative feedback mechanism that suppresses the protrusive/adhesion activities elsewhere. Such a coordination mechanism may be impaired in transformed cells, due to defects in signal transduction. Previous studies have suggested potential interactions between signaling pathways mediated by H-ras and the small GTP-binding proteins, including rac and rho, which are known to modulate both actin organization and myosin II contractility (Narumiya et al., 1997; Hall, 1998; Rottner et al., 1999). In addition, H-ras may disrupt the state of protein tyrosine phosphorylation, particularly the focal adhesion kinase (FAK) and paxillin, which are associated with focal adhesion and believed to play a role in regulating adhesion-activated transmembrane signals (Parsons, 1996; Ilic et al., 1997).

In addition to cell migration, traction forces are likely to play a role in the loss of growth regulation in transformed cells. The exertion of active traction stresses induces strains and hence structural modifications within the cell-substratum linkages, the cell membrane, or the cytoskeleton. These structural changes could in turn modulate the catalytic activity of enzymes, the susceptibility of substrates, and/or the conductance of ion channels (Boudreau and Jones, 1999; Giancotti and Ruoslahti, 1999; Gumbiner, 1996; Katz and Yamada, 1997; Schoenwaelder and Burridge, 1999; Schwartz and Baron, 1999). Accumulating evidence from mechanical stimulation and fluid shear experiments indicates that mechanical forces can affect gene expression, cell cycle, and apoptosis (Sadoshima and Izumo, 1993; Davies, 1995; Schwartz and Baron, 1999; Grinnell et al., 1999). By exerting weaker, disorganized forces to the substrate, PAP2 cells would also receive weaker, disorganized mechanical input and respond with altered growth behavior (Lukashev and Werb, 1998). Although the pathways leading to altered motility and loss of growth control are likely different, the common root in mechanical interactions explains why the two are usually coupled in cancerous transformation.

The capacity of cells to use traction forces for the regulation of motility and growth bear far-reaching implications on such biological phenomenon as contact inhibition, wound healing, and development. Future studies utilizing this novel traction force mapping technique will serve to further our understanding of the mechanical interaction between cells and their environment as well as the impact of this interaction on a wide spectrum of cellular functions.

We thank Dr. Ann Chambers, London Regional Cancer Center, Ontario, Canada, for the generous supply of NIH 3T3 and PAP2 cells; Boston University Center for Scientific Computing for the use of supercomputer facilities; and Dr. K. Beningo for helpful critiques and suggestions.

This project was supported by National Institutes of Health research grants GM-32476 to Y.-L.W. and GM-61806 to M.D. S.M. is supported by a National Institutes of Health NRSA predoctoral fellowship GM-20749.

REFERENCES

Albrecht-Buehler, G. 1980. Autonomous movement of cytoplasmic fragments. *Proc. Natl. Acad. Sci. U.S.A.* 77:6639–6643.

Bondy, G. P., S. Wilson, and A. F. Chambers. 1985. Experimental metastatic ability of H-ras transformed NIH 3T3 cells. *Cancer Res.* 45: 6005–6009.

Boudreau, N. J., and P. L. Jones. 1999. Extracellular matrix and integrin signaling: the shape of things to come. *Biochem. J.* 339:481–488.

Brown, F. A., V. Dugina, A. G. Dunn, and M. J. Vasiliev. 1989. A quantitative analysis of alterations in the shape of cultured fibroblasts induced by tumor-promoting phorbol ester. *Cell Biol. Int. Rep.* 13: 357–366.

Burton, K., P. H. Jung, and L. D. Taylor. 1999. Keratocytes generate traction forces in two phases. *Mol. Biol. Cell.* 10:3745–3769.

Burton, K., and L. D. Taylor. 1997. Traction forces of cytokinesis measured with optically modified elastic substrata. *Nature.* 385:450–454.

Byers, H. R., T. Etoh, R. J. Doherty, J. A. Sober, and C. M. Mihm. 1991. Cell migration and actin organization in cultured human primary, recurrent cutaneous and metastatic melanoma. *Am. J. Pathol.* 139:423–435.

Davies, P. F. 1995. Flow-mediated endothelial mechanotransduction. *Physiol. Rev.* 75:519–560.

Dembo, M., and Y.-L. Wang. 1999. Stresses at the cell-to-substrate interface during locomotion of fibroblasts. *Biophys. J.* 76:2307–2316.

Depasquale, A. J., and S. C. Izzard. 1987. Evidence for an actin containing cytoplasmic precursor of the focal contact and the timing of incorporation of vinculin at the focal contact. *J. Cell Biol.* 105:2803–2809.

DiMilla, P. A., K. Barbee, and D. A. Lauffenburger. 1991. Mathematical model for the effects of adhesion and mechanics on cell migration speed. *Biophys. J.* 60:15–37.

Egan, S. E., G. A. McClarty, L. Jarolim, J. A. Wright, I. Spiro, G. Hager, and A. H. Greenberg. 1987. Expression of H-ras correlates with metastatic potential: evidence for direct regulation of the metastatic phenotype in 10T1/2 NIH 3T3 cells. *Mol. Cell. Biol.* 7:830–837.

Elson, E. L., S. F. Felder, P. Y. Jay, M. S. Kolodney, and C. Pasternak. 1997. Force in cell locomotion. *In* Biochemical Society Symposium, Vol. 65. J. M. Lackie, G. A. Dunn, and G. E. Jones, editors. Oxford, UK.299–314.

Galbraith, C. G., and M. P. Sheetz. 1997. A micromachined device provides a new bend on fibroblast traction forces. *Proc. Natl. Acad. Sci. U.S.A.* 94:9114–9118.

Galbraith, C. G., and M. P. Sheetz. 1998. Forces on adhesive contacts affect cell function. *Curr. Opin. Cell Biol.* 10:566–571.

Giancotti, F. G., and E. Ruoslahti. 1999. Integrin signaling. *Science.* 285:1028–1032.

Goldschmidt-Clermont, P. J., R. M. Galbraith, D. L. Emerson, F. Marsot, A. E. Nel, and P. Arnaud. 1985. Distinct sites on the G-actin molecule bind group-specific component and deoxyribonuclease I. *Biochem. J.* 228:471–477.

Grinnell, F., M. Zhu, M. A. Carlson, and J. M. Abrams. 1999. Release of mechanical tension triggers apoptosis of human fibroblasts in a model of regressing granulation tissue. *Exp. Cell Res.* 248:608–619.

Gumbiner, B. M. 1996. Cell adhesion: the molecular basis of tissue architecture and morphogenesis. *Cell.* 84:345–357.

Hall, A. 1998. Rho GTPases and the actin cytoskeleton. *Science.* 279: 509–514.

Harris, A. K., D. Stopak, and P. Wild. 1981. Fibroblast traction as a mechanism for collagen morphogenesis. *Nature.* 290:249–251.

Harris, A. K., P. Wild, and D. Stopak. 208. 1980. Silicone rubber substrata: a new wrinkle in the study of cell locomotion. *Science.* 177–179.

Heath, J. P. 1983. Behavior and structure of the leading lamella in moving fibroblasts. *J. Cell Sci.* 60:331–354.

Hill, S. A., S. Wilson, and A. F. Chambers. 1988. Clonal heterogeneity, experimental metastatic ability, and p21 expression in H-ras-transformed NIH 3T3 cells. *J. Natl. Cancer Inst.* 80:484–490.

Ilic, D., C. H. Damsky, and T. Yamamoto. 1997. Focal adhesion kinase: at the crossroads of signal transduction. *J. Cell Sci.* 110:401–407.

Ishihara, A., B. Holifield, and K. Jacobson. 1988. Analysis of lateral redistribution of a plasma membrane glycoprotein- monoclonal antibody complex. *J. Cell Biol.* 106:329–343.

Katz, B. Z., and K. M. Yamada. 1997. Integrins in morphogenesis and signaling. *Biochimie.* 79:467–476.

Lauffenburger, D. A., and A. F. Horwitz. 1996. Cell migration: a physically integrated molecular process. *Cell.* 84:359–369.

Leader, W. M., D. Stopack, and A. K. Harris. 1983. Increased contractile strength and tightened adhesions to the substratum result from reverse transformation of cho cells by dibutyryl cyclic adenosine monophosphate. *J. Cell Sci.* 64:1–11.

Lee, W. M., and R. M. Galbraith. 1992. The extracellular actin-scavenger system and actin toxicity. *N. Engl. J. Med.* 326:1335–1341.

Li, Y., Z. Hu, and C. Li. 1993. New method for measuring Poisson's ratio in polymer gels. *J. Appl. Polymer Sci.* 50:1107–1111.

Lukashev, M. E., and Z. Werb. 1998. ECM signaling: orchestrating cellular behavior and misbehavior. *Trends Cell Biol.* 8:437–441.

Malawista, S. E., and A. DeBoisefleury-Chevance. 1982. The cytokinetoplast: purified, stable, and functional motile machinery from human blood polymorphonuclear leukocytes. *J. Cell Biol.* 95:950–973.

Narumiya, S., T. Ishizakit, and N. Watanabe. 1997. Rho effectors and reorganization of actin cytoskeleton. *FEBS Lett.* 410:68–72.

Oliver, T., M. Dembo, and K. Jacobson. 1999. Separation of propulsive and adhesive traction stresses in locomoting keratocytes. *J. Cell Biol.* 145:589–604.

Oliver, T., K. Jacobson, and M. Dembo. 1998. Design and use of substrata to measure traction forces exerted by cultured cells. *Methods Enzymol.* 298:497–521.

Parsons, J. T. 1996. Integrin-mediated signaling: regulation by protein tyrosine kinases and small GTP-binding proteins. *Curr. Opin. Cell Biol.* 8:146–152.

Pelham, R. J., and Y.-L. Wang. 1999. High resolution detection of mechanical forces exerted by locomoting fibroblasts on the substrate. *Mol. Biol. Cell.* 10:935–945.

Radmacher, M., R. W. Tillmann, M. Fritz, and H. E. Gaub. 1992. From molecules to cells: imaging soft samples with the atomic force microscope. *Science.* 257:1900–1905.

Rottner, K., A. Hall, and V. J. Small. 1999. Interplay between rac and rho in the control of substrate contact dynamics. *Curr. Biol.* 9:640–648.

Sadoshima, J.-I., and S. Izumo. 1993. Mechanical stretch rapidly activates multiple signal transduction pathways in cardiac myocytes: potential involvement of an autocrine/paracrine mechanism. *EMBO J.* 12: 1681–1692.

Schoenwaelder, S. M., and K. Burridge. 1999. Bidirectional signaling between the cytoskeleton and integrins. *Curr. Opin. Cell Biol.* 11: 274–286.

Schwartz, M. A., and V. Baron. 1999. Interactions between mitogenic stimuli, or, a thousand and one connections. *Curr. Opin. Cell Biol.* 11:197–202.

Sheetz, M. P., D. P. Felsenfeld, and G. C. Galbraith. 1998. Cell migration: regulation of force on extracellular matrix-integrin complexes. *Trends Cell Biol.* 8:51–54.

Shin, Y.-E., J.-Y. Lee, M.-K. Park, G.-B. Heong, E.-G. Kim, and S.-Y. Kim. 1999. H-ras is a negative regulator of $\alpha 3\beta 1$ integrin expression in ECV304 endothelial cells. *Biochem. Biophys. Res. Commun.* 257:95–99.

Small, V. J., K. Rottner, I. Kaverina, and K. I. Anderson. 1998. Assembling an actin cytoskeleton for cell attachment and movement. *Biochim. Biophys. Acta.* 1404:271–281.

Svitkina, T. M., A. B. Verkhovsky, K. M. McQuade, and G. G. Borisy. 1997. Analysis of the actin-myosin II system in fish epidermal keratocytes: mechanism of cell body translocation. *J. Cell Biol.* 139: 397–415.

Van Baelen, H., R. Bouillon, and P. D. Moor. 1980. Vitamin D-binding protein (Gc-globulin) binds actin. *J. Biol. Chem.* 255:2270–2272.

Varani, J., E. Suzanne, G. Fligiel, and B. Wilson. 1986. Motility of rasH oncogene transformed NIH-3T3 cells. *Invest. Metastasis.* 6:335–346.

Verkhovsky, A. B., T. M. Svitkina, and G. G. Bosisy. 1999. Self-polarization and directional motility of cytoplasm. *Curr. Biol.* 9:11–20.

Wang, Y.-L. 1985. Exchange of actin subunits at the leading edge of living fibroblasts: possible role of treadmilling. *J. Cell Biol.* 101:597–602.

Wang, Y.-L., and R. J. Pelham. 1998. Preparation of a flexible, porous polyacrylamide substrate for mechanical studies of cultured cells. *Methods Enzymol.* 298:489–496.